

# Keys to Accurate Feature Extraction Using Residual Spiking Neural Networks

Alex Vicente-Sola <sup>\*†</sup>, Davide L. Manna <sup>†</sup>, Paul Kirkland <sup>†</sup>, Gaetano Di Caterina <sup>†</sup>, and Trevor Bihl <sup>‡</sup>

## Abstract

Spiking neural networks (SNNs) have become an interesting alternative to conventional artificial neural networks (ANN) thanks to their temporal processing capabilities and their low-SWaP (Size, Weight, and Power) and energy efficient implementations in neuromorphic hardware. However the challenges involved in training SNNs have limited their performance in terms of accuracy and thus their applications. Improving learning algorithms and neural architectures for a more accurate feature extraction is therefore one of the current priorities in SNN research. In this paper we present a study on the key components of modern spiking architectures. We empirically compare different techniques in image classification datasets taken from the best performing networks. We design a spiking version of the successful residual network (ResNet) architecture and test different components and training strategies on it. Our results provide a state of the art guide to SNN design, which allows to make informed choices when trying to build the optimal visual feature extractor. Finally, our network outperforms previous SNN architectures in CIFAR-10 (94.1%) and CIFAR-100 (74.5%) datasets and matches the state of the art in DVS-CIFAR10 (71.3%), with less parameters than the previous state of the art and without the need for ANN-SNN conversion. Code available at [https://github.com/VicenteAlex/Spiking\\_ResNet](https://github.com/VicenteAlex/Spiking_ResNet)

## 1 Introduction

Artificial Neural Networks (ANNs) have achieved in recent years unprecedented performances in many computer vision tasks. However, these artificial systems still cannot be compared to a real brain in terms of robustness, energy consumption or generalization capabilities. Therefore, as an attempt to imitate more of the valuable properties of brains, artificial Spiking Neural Networks (SNNs)

have been proposed as an alternative to conventional ANNs. SNNs closely replicate the functioning of biological neurons, allowing for sparse asynchronous computations and time-dependent neuronal functionality. The full potential of these properties is yet to be explored, but it has already been proved how substantial improvements in energy efficiency can be obtained by implementing SNNs in neuromorphic hardware [1, 2], bringing efficiency gains of up to 100 times less compared to standard ANNs in CPU/GPU hardware [3]. Given the ever increasing network size and power demands of standard ANNs, such energy efficiency gains are of particular interest as they allow to reduce SWaP (Size, Weight, and Power) for energy efficiency operations [4].

However, training SNNs is a more challenging task than training regular non-spiking networks. Non-spiking ANNs owe most of their success to the back-propagation of error (BP) algorithm [5], but in the case of SNNs the spiking behaviour inside the neurons creates a non-differentiable function, hindering the application of BP. Moreover the time dependencies of the neuronal states add extra complexity to the credit assignment calculations. These drawbacks result, in most cases, in SNNs having a lower final accuracy than regular ANNs.

In order to overcome the aforementioned challenges, some approaches use conversion methods [6, 7, 8], where they train non-spiking ANNs and then approximate their computations using an SNN. Compared to directly training an SNN, these methods have higher latency and energy consumption, they are not able to perform online learning and lose temporal resolution. This is why improving directly trained SNNs is still a necessity.

Direct training can be performed through bio-plausible unsupervised methods such as Spike-timing-dependent plasticity (STDP), but when ground truth is available for the task to solve, supervised learning through surrogate gradient BP [9] is the best performing method. In this work we focus on the latter.

In order to improve the feature extraction process of SNNs in visual tasks, in this paper we present a study on the key components of modern spiking architectures, such as the topology, residual connections, batch normalization strategies, boosting methods, hyper-parameter optimization

<sup>\*</sup>Corresponding author: alex.vicente-sola@strath.ac.uk

<sup>†</sup>Neuromorphic Sensor Signal Processing Lab, Centre for Image and Signal Processing, Electrical and Electronic Engineering, University of Strathclyde, Glasgow, UK.

<sup>‡</sup>Air Force Research Laboratory, Wright Patterson AFB, OH

or fine-tuning. The conclusions inferred from our experiments allow us to build a new SNN architecture that outperforms the best reported accuracies in the CIFAR-10 and CIFAR-100 datasets, and achieves comparable results in DVS-CIFAR10. These results prove how directly training SNNs can already outperform conversion methods, allowing to exploit all the benefits of spiking computations without compromising accuracy. Additionally, the lessons learned from our experiments can also be valuable for those designing new SNN feature extractors in the future.

## 2 Related work

As mentioned in the previous section, one limitation in implementing SNNs is the difficulty to train them. Conventional gradient descent algorithms are not directly applicable given the intrinsic presence of non-differentiable spiking functions, as a result, different workaround strategies have been proposed. These strategies can be mainly categorized into two groups, ANN to SNN conversion methods and direct training methods. In this section, we overview the state of the art of this two approaches.

### 2.1 Conversion methods

In order to overcome the challenges in SNN training and to obtain the most accurate SNN systems, many works have adopted conversion approaches. These methods allow to bypass the training challenges of SNNs by training a non-spiking ANN and then transforming it to spiking format. This transformation reconstructs each of the neurons in the original network using spiking neurons, therefore the key challenge is to represent continuous activation values using the binary outputs of spiking neurons.

Most of these techniques are based on rate-based conversion [6, 7, 10], where the network is set up such that the spiking frequency of the converted neuron is proportional to the activation value of the original one. These methods can only convert ANNs using the Rectified Linear Unit (ReLU) activation function. In order to reduce the energy cost of these conversions, Temporal-SwitchCoding (TSC) [11] was proposed, where the activation value is encoded in the latency of spiking rather than the frequency.

Alternatively, other approaches such as [8, 12] can be applied to any type of network. The first one manages to do this by using circuits of neurons in order to approximate arbitrary functions. The second one does the same by using FS-neurons, a parametric neuron model that can be optimized to approximate any function.

Converted networks can be implemented in energy efficient neuromorphic hardware; however, forcing the SNN to imitate non-spiking computations makes it lose some of its

properties. Compared to a directly trained SNN, the converted one will have higher latency and energy consumption and will not be able to perform online learning. Moreover it will have a lower temporal resolution, which is likely to cause under-performance when processing neuromorphic data as proved by [13].

### 2.2 Direct training

Directly training the SNN without conversion allows one to exploit all its valuable properties; however, the challenge becomes then to successfully train it given that gradient descent based methods can not be applied to non-differentiable spiking functions. The most common strategy in state of the art methods is the use of surrogate gradients [14, 15], a method where the spiking function is used in the forward path, but when calculating its derivative in the backwards path, a continuous tractable function is used, which tries to approximate the behaviour of the real derivative.

Another option is to use a version of the SNN model that is directly differentiable. Some examples can be found in [9]. We can find models using soft non-linearities [16], probabilistic models [17] or latency-based networks [18].

Alternatively, supervised learning can also be performed without the differentiation of the whole network. Some examples use local approaches with algorithms such as [19], where the loss is computed locally in each neuron, or by using three factor learning rules [20].

Depending on the needs of the system, the optimal learning method might change, but when talking about final task accuracy, surrogate gradient BP is the best performing method so far. All the best SNN feature extractors consistently use this method, but the BP implementations and the surrogate functions they use vary between them.

Concerning the BP implementation, different variations can be found among the best performing networks. Some works such as [15] choose to simply unroll the network in time and use Back-propagation Through Time (BPTT). A slightly different implementation is found in [21], where the authors use a Spike-based BP algorithm which proposes a novel way of accounting for the leak factor of LIF neurons. Finally, there are also BP approaches where the input spikes are convolved with spike response kernels like in [22], which allows for convenient spike response implementations at the cost of saving more spike time-stamps in memory.

For the surrogate functions, there is no consensus either. We find triangle shape surrogates in [15], rectangular shaped in [23], and arc-tangent shaped in [24, 25].

## 2.3 SNN architectures

Regarding the state of the art of SNN topologies, literature usually measures their feature extraction capabilities by assessing their image classification accuracy in public datasets. In the present day, among directly trained networks, the highest accuracies are reported for networks basing their topologies on VGG [26] and ResNet [27] architectures.

In non-spiking deep learning, after the development of deep feed-forward networks such as VGG, the next big improvement came with the addition of residual connections. As demonstrated in [27], residual connections allowed to successfully train much deeper architectures, giving rise to a more accurate and efficient family of networks.

The reason for this improved performance is that residual connections help alleviate the problem of depth-induced accuracy degradation. Without residual connections, when increasing the depth of the network, the accuracy firstly saturates, but then it degrades rapidly. This is caused by the fact that extra layers increase the complexity of the problem to optimize, therefore it can get to a point where the benefit of adding extra layers does not compensate the harm of increasing optimization difficulty.

The way residual networks solve this problem is by making the network easier to optimize. Given an input  $x$  and the mapping function of a layer  $F(x)$ , the output of a layer with a residual connection will be:

$$H(x) = F(x) + x \quad (1)$$

Then, the residual mapping  $F(x) = H(x) - x$  should become easier to optimize than the original  $F(x) = H(x)$ . Moreover, an identity mapping  $H(x) = x$  can be accomplished just by setting the weights in the layer to zero ( $F(x) = 0$ ), allowing the network to easily ignore unnecessary layers, and therefore not degrading the result.

In order to port these benefits to SNN, Lee et al. [21] Zheng et al. [23] and Fang et al. [25] implement the first trainable spiking ResNets, managing to train deeper networks than VGGs and achieving competitive results. On the other hand, [15, 24] implement VGG-like architectures which are shallower, but larger in number of parameters. These non-residual feed-forward networks still outperform the aforementioned ResNets in many datasets (see Table 11 in Section 5).

## 3 Methods

### 3.1 Spiking neuron model

In order to perform their computations, SNNs simulate the behaviour of biological neurons by means of mathematical models.

In this work we use the Leaky Integrate-and-Fire (LIF) model [28]. Despite their simplicity, LIF neurons found great success in many state of the art systems.

The LIF model can be formulated as the differential equation seen in Eq. 2, where  $U(t)$  is the membrane potential,  $U_{rest}$  the resting potential,  $\tau$  is the time constant and  $I(t)$  is the input current. When the voltage  $U(t)$  surpasses a set threshold  $U_{th}$ , the neuron emits a spike and the potential is reset by subtraction.

$$\tau \frac{du}{dt} = -(U(t) - U_{rest}) + RI(t) \quad (2)$$

In order to easily program this behaviour in machine learning models, explicit iterative versions of this differential equation are used. Let  $i$  be a post-synaptic neuron,  $u_{i,t}$  is its membrane potential,  $o_{i,t}$  its spiking activation and  $\lambda$  the leak factor. The index  $j$  belongs to the pre-synaptic neuron and the weights  $w_{i,j}$  dictate the value of the synapses between neurons. Then, the iterative update of the neuron activation is calculated as follows:

$$o_{i,t} = g \left( \sum_j (w_{ij} o_{j,t}) + \lambda \cdot u_{i,t-1} \right) \quad (3)$$

where  $g(x)$  is the thresholding function, which converts voltage to spikes:

$$g(x) = \begin{cases} 1, & \text{if } x \geq U_{th} \\ 0, & \text{if } x < U_{th} \end{cases} \quad (4)$$

After spiking, a reset is performed by the subtraction  $u_{i,t}^* = u_{i,t} - U_{th}$ , where  $u_{i,t}^*$  is the membrane potential after resetting.

### 3.2 Spiking Residual Network

With the objective of building the most accurate SNN feature extractor, our starting point is to implement a spiking residual network (S-ResNet).

The motivation to choose this architecture is that almost all the non-spiking state of the art ANNs make use of residual connections in order to allow for the training of very deep networks. On the contrary, in the SNN domain, the state of the art is still based in VGG-like architectures for datasets such as CIFAR-10, CIFAR-100 and DVS-CIFAR10. Therefore we define a new S-ResNet that will allow to outperform the previous state of the art and justify the use of residual connections also in the SNN domain.

#### 3.2.1 Implementation of a Spiking residual connection

In order to design our S-ResNet, the first step is to define the spiking residual implementation. The skip connection

in a non-spiking network just sums the activation value of a previous layer to the activation of the current one, but in spiking format; this sum can be performed in three different ways:

- **Membrane to membrane (M2M):** The membrane potential of layer  $a$  is directly summed to the membrane potential of layer  $b$ . This enforces an identity mapping of the voltage state, but if the thresholds are different between layers  $a$  and  $b$ , the spiking output will be different (see red connection in Fig. 1).
- **Spike output to membrane (S2M):** The spiking output of layer  $a$  feeds the membrane potential of neurons in layer  $b$ . This is the most intuitive and biologically plausible solution, but it can fail to fulfil the purpose of the original residual connections. In case of layer  $a = 0$ , it will only implement an identity mapping if the spikes transmitted through the residual connection communicate a voltage greater than or equal to the neuron threshold. In any other case, the final activations would be different from those at the input. This kind of connection is used in [21, 23] (see green connection in Fig. 1).
- **Spike output to spike output (S2S):** The spiking output of layer  $a$  is summed to the spiking output of layer  $b$ . This connection will implement an identity mapping if layer  $b$  contains no extra information, as it bypasses the problem of applying thresholding at each layer, and it can propagate it through the network unchanged. This kind of connection is used in [25] (see purple connection in Fig. 1).

In S2S implementations, as we are combining the signals using a sum, if both of the connected neurons are active, the final result will be a double activation of the neuron. In practice this is not a problem as it could still be computed in neuromorphic hardware. Still, as proposed in [25], the connection can also be defined with an OR gate, avoiding double spikes. In practice, S2M connections, when implemented with a residual synapse weight equal or greater than the threshold, can be considered equivalent to an S2S connection with OR gate if the network uses hard reset after spikes.

For this work we choose the S2S implementation, as it is the most straightforward implementation of residual identity mappings, and therefore it will ensure that we gain the full benefits of this kind of connections.

### 3.2.2 Network topology

With the residual connection implementation defined, the following choice to be made is the global network architecture. In the non-spiking domain it has already been proven

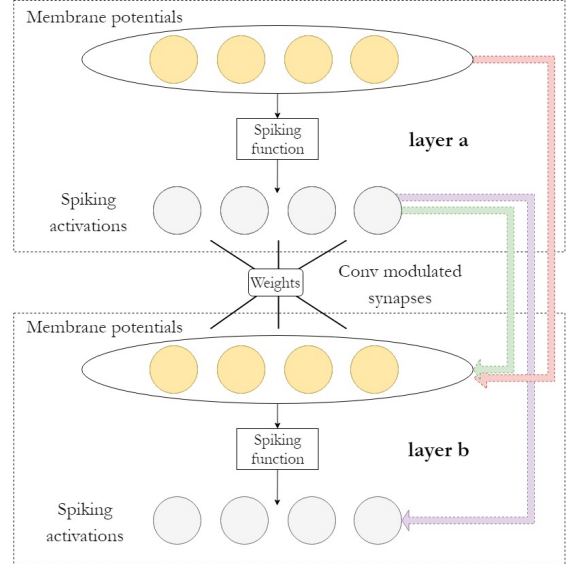


Figure 1. The three possible residual connections in an SNN. In red: Membrane to membrane connection. Purple: Spike output to spike output. Green: Spike output to membrane. Note that the layers are displayed in one dimensional fashion for simplicity, but it is equivalent to a three dimensional convolutional map if the synapses are defined by a convolutional layer.

Table 1. Table defining the CNN architecture of the original ResNet proposed for the CIFAR datasets. The variable  $n$  allows to control the depth of the network.

output map size	32x32	16x16	8x8
# layers	1+2n	2n	2n
# filters	16	32	64

how the original ResNet architecture [27] outperforms feed-forward architectures without residuals; therefore, in order to test if the same principles apply to SNN, the obvious choice is to reuse the same topology.

Depending on the resolution and complexity of the dataset to target, the optimal architecture can vary; that is why in [27] the architecture used for the ImageNet dataset and for CIFAR-10 are different. CIFAR images have a resolution of 32x32, while the images are 224x224 for ImageNet (after resizing), meaning that more downsampling operations will be needed in the second one in order to have a comparable receptive field. As we are targeting CIFAR-10, CIFAR-100 and DVS-CIFAR10, we will base our global network architecture on the smaller ResNet proposed for these datasets. The architecture is defined in [27] in a table, such as Table 1.

Regarding the batch normalization (BN) layers in the architecture, regular BN can be used in an SNN, but improved performance has been reported by using Batch Normalization Through Time (BNTT) [15], a time-varying BN that learns different statistics for each time-step. This is consistent with the studies performed in non-spiking RNNs, where works such as [29] argue that the statistics of different time-steps can differ significantly. For that reason, in our final architecture we use BNTT. As further proof, Table 2 in Section 4 demonstrates the performance gains of using BNTT compared to regular BN. A diagram of the final architecture can be found in Fig. 2.

To the best of our knowledge, this work is the first to implement the aforementioned architecture for SNN training. [21, 23] implement customized version with extra fully connected layers and larger amounts of channels in convolutional layers (see the difference in parameters in Fig. 3 in Section 5). [25] implements ResNet’s ImageNet version as they target that dataset. Moreover these three works use time averaged statistics for their BN strategies, while we use BNTT.

### 3.2.3 Boosting strategies

Boosting techniques allow to combine the predictions of multiple weak classifiers to create a stronger one. Previous work in SNNs [24] has already applied simple versions of this strategy by converting the classification layer into a voting layer.

We tested the same approach as [24] and adapted the last fully-connected to have  $10 \times C$  neurons, where  $C$  is the number of classes. Then an average pooling layer of kernel size 10 and stride 10 reduces the dimension back to the number of classes  $C$ . This process computes the score of each class as the average of 10 neuron states, which can be seen as a voting scheme for 10 different sub-networks.

In Section 4, Tables 3 and 4 demonstrate the effects of adding the boosting layer. Some networks provided improved performance when using this strategy, while others did not, so we keep this layer only in those cases where it is beneficial. In our final results, only the CIFAR-10 network uses it.

### 3.3 Training framework

Our network is trained to perform image classification through supervised learning. In order to allow for this classification, the last neuron layer is defined with no leak and cannot spike. Then the voltage accumulated in the layer after  $T$  time-steps divided by  $T$  is considered the output value.

The output class scores are compared to the ground truth by means of a cross-entropy loss (Eq. 5), where  $C$  is the

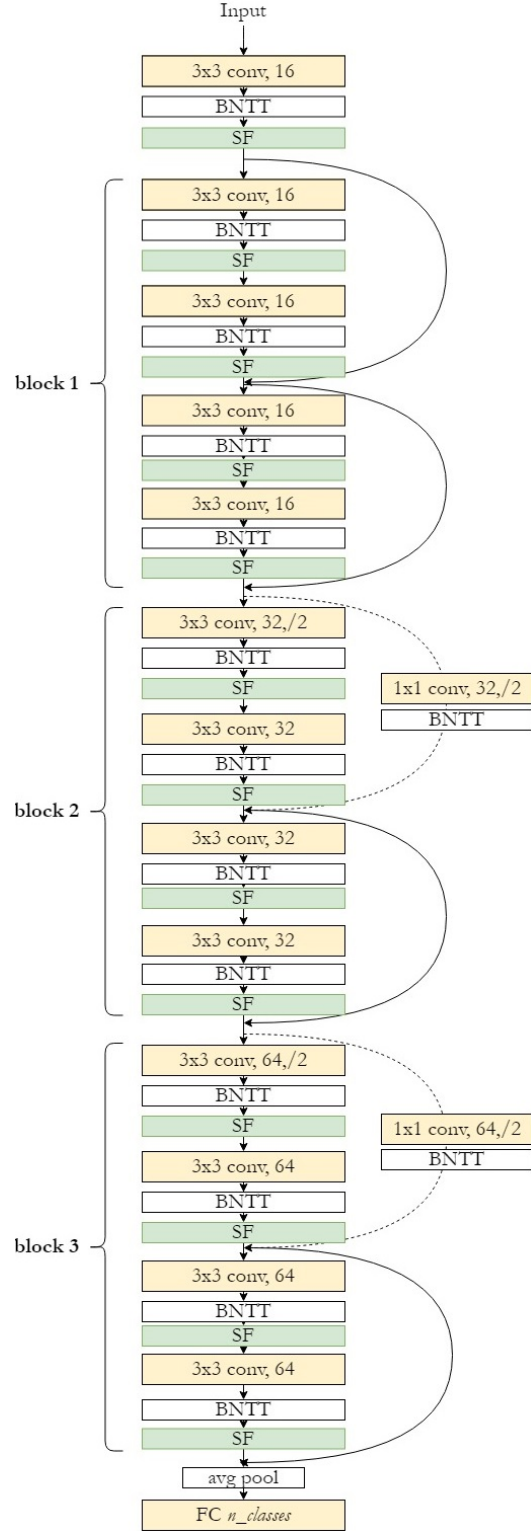


Figure 2. Example architecture for an S-ResNet with  $n = 2$  and 16 base filters. SF stands for spiking function.

number of classes,  $u_{i,T}$  the voltage of neuron  $i$  after the last time-step, and  $y_i$  are the ground truth labels:

$$L = - \sum_i^C y_i \log\left(\frac{e^{u_{i,T}}}{\sum_j^C e^{u_{j,T}}}\right) \quad (5)$$

With the loss defined, the weight updates for the learning process are calculated through BPTT.

The final voltage at each layer is dependent of the contribution of all previous time-steps, therefore the derivative of the loss function with respect to the network weights can be defined as the sum in Eq. 6.

$$\frac{\partial L}{\partial w_{i,j}} = \sum_{t=1}^T \frac{\partial L}{\partial u_{t,i}} \frac{\partial u_{t,i}}{\partial p_{t,i}} \frac{\partial p_{t,i}}{\partial w_{i,j}} \quad (6)$$

where  $p_{i,t}$  is the current transmitted through the synapses after applying the weights:

$$p_{i,t} = \sum_j w_{i,j} o_{j,t} \quad (7)$$

Then using the chain rule, the dependencies of the term  $\frac{\partial L}{\partial u_{t,i}}$  can be unraveled:

$$\frac{\partial L}{\partial u_{t,i}} = \frac{\partial L}{\partial o_{t,i}} \frac{\partial o_{t,i}}{\partial u_{t,i}} + \frac{\partial L}{\partial o_{t+1,i}} \frac{\partial o_{t+1,i}}{\partial u_{t,i}} \quad (8)$$

Notice that  $\frac{\partial o_{t,i}}{\partial u_{t,i}}$  requires to compute the derivative of the thresholding function, which is non-differentiable. We solve this by using a triangle shaped surrogate gradient. As in [15], we set  $\alpha = 0.3$ .

$$\frac{\partial o_{t,i}}{\partial u_{t,i}} = \alpha \max\{0, 1 - u_{t,i}\} \quad (9)$$

In practice this can be easily implemented using auto-differentiation tools such as Pytorch [30].

### 3.4 Input preprocessing

**Frame-based datasets:** Frame-based images need to be encoded into spikes in order for an SNN to process them. Works like [15] use a Poisson spike generation process which transforms the image frame into a sequence of spikes. Other works [24, 23] feed the unprocessed frame to the first SNN layer, making the pixel intensity equivalent to a constant input voltage for the first neurons.

The latter allows for better results, as all of the information is presented at each time-step, while the former will require many steps to represent all of the information and will add variability to the data. Still, we believe using a spike generation process is a better representation of a scenario where the input data is spiking information (such as the data coming from event cameras), so choosing one method

or another should depend on the objective of our simulation. Therefore in this work we use both approaches in order to compare results. Our best performing networks are trained without Poisson encoder in order to maximize accuracy. Additionally, images are always normalized with respect to the statistics of the dataset.

**Neuromorphic datasets:** Data produced by neuromorphic cameras represent the changes in the scene, and these are often presented in event format. An event is a discrete package of information indicating location, time-stamp and polarity (i.e. change in brightness).

We use the events to build frames containing spiking activations. Such frames have two channels, one for positive polarity and one for negative, and they accumulate all events occurring in a time window. The size of the time window is defined by the amount of time-steps we want to have for each sequence. We implement this process using the SpikingJelly library [31].

**Data augmentation:** All datasets are augmented using random horizontal flips and random crops.

### 3.5 Hyper-parameters

The performance of the proposed network depends on certain hyper-parameters, such as the leak factor of the membrane, the number of time-steps or the learning rate for training. The optimal value of these parameters varies depending on the architecture of the network, the training procedure and the task at hand. That is why in order to properly asses how useful an architecture or a training method is, we first need to find its optimal hyper-parameter setup.

We address this challenge by using BOHB [32], a hyper-parameter optimization technique that combines Bayesian Optimization (BO) and Hyperband (HB), a multi-armed bandit strategy. Using this method, we optimize the hyper-parameters for S-ResNet38 in the CIFAR-100 dataset. The learning rate for this training is divided by 10 at 50%, 70% and 90% of the training process. The resulting hyper-parameters are also used for the rest of networks and datasets, as with the hardware available we could not afford to run an individual search per setup.

The best performing parameters are:  $leak = 0.874$ ,  $time-steps = 50$ ,  $learning\ rate = 0.0268$ .

Notice that the target of the search was only to optimize accuracy, therefore the amount of time-steps tends to be maximized as it has a monotonically non-decreasing relationship with the accuracy. Section 5.2 demonstrates the effects of reducing the amount of time-steps.

## 4 Experiments

In order to maximize the accuracy of our method, we conducted a search for the key components in state of the

art architectures that allow for improved performance. In this section we present empirical results obtained from testing these components in our networks. The results from these comparisons allow us to compose a network which outperforms previous approaches in multiple datasets.

**Batch normalization strategies:** We compare performances using time-dependent BN statistics versus time averaged statistics. Table 2 shows how BNTT outperforms regular BN for the same network.

**Boosting layer:** As introduced in Section 3.2.3, a simple boosting layer can improve the accuracy of the system in some cases. Tables 3 and 4 show the effect of this component in the accuracy our networks. In the CIFAR-10 datasets the accuracy is improved by using this technique, while in the CIFAR-100 one, where we have more classes, increasing the size of the last fully connected in order to perform boosting ends up being detrimental.

**Parametric Leaky Integrate and Fire:** The authors in [24] propose to learn the leak coefficient of the LIF neurons directly through back-propagation as another parameter of the network. By doing this they can also afford to learn a different leak value for each layer. They call this method the Parametric Leaky integrate-and-fire (PLIF) neuron. Table 5 shows our results after training S-ResNet38 with PLIF and with a single leak coefficient learned through hyper-parameter search.

We do not achieve our best results using the PLIF neuron, still, we believe this strategy is a very efficient way of finding this hyper-parameter. For this reason, we test it again for the search of a shared leak value instead of calculating a different one per layer. Table 6 shows the difference between the leak value found through hyper-parameter search and the one found by back-propagation. It is interesting to see how the two values differ by a considerable amount, having the one found by back-propagation a slower leakage than the one found through the BOHB method.

Still, both values perform well when the network adapts its weights to work with them. The performance comparison between them can be found in Table 7, where we compare our network trained with the BOHB optimized value to an identical network which learned the shared leak value through PLIF.

**Spike generation for frame based datasets:** As mentioned in Section 3.4, when working with frame based datasets, we tested two different methods for the spike encoding process. One consists in transforming the intensity values into spikes by means of a Poisson spike generation process. The other consists in transforming them by means of the first convolutional layer (i.e. feeding the raw image to the network).

As expected, the results in Table 8 show how encoding by means of the first convolutional layer gives a better result than generating spikes as a Poisson process. In order to

Table 2. Image classification test performance on CIFAR-100. Except for the batch normalization module, both architectures and training procedures are identical. Trained for 100 epoch.

Network	CIFAR-100 Accuracy
VGG11-SNN BNTT	65.2 %
VGG11-SNN BN time averaged	62.0 %

Table 3. Image classification test performance on CIFAR-10. S-Resnet38 stands for the architecture defined in Section 3.2.2 with  $n = 6$  and 16 base filters. Wider architectures use 32 base filters and "boosting" indicates the use of a boosting layer (Section 3.2.3). Wider architectures trained for 70 epochs, regular architectures trained for 200 epochs.

Network	Parameters	CIFAR-10 Acc
S-ResNet38	634,000	90.82 %
S-ResNet38 + boosting	639,760	92.00 %
S-ResNet38_wider	2,388,256	92.66 %
S-ResNet38_wider + boosting	2,399,776	93.77 %

maximize accuracy, for the rest of our experiments we use the encoding by convolution approach.

**Extra training data:** In the deep learning domain, most state of the art performances in computer vision are achieved by means of fine tuning. This strategy consists in taking a network that has already been trained in a different dataset and then training it further for the task at hand. In the visual domain this strategy works well, as visual data has many transferable features.

We test this strategy by pre-training our networks with CIFAR-100 and then fine-tuning for DVS-CIFAR10 and CIFAR-10. The results are presented in Table 9 and Table 10. We obtain higher accuracy results in all cases but for the larger S-ResNet in CIFAR-10. Moreover these trainings converge faster, making it a great solution for any further work building on top of these feature extractors. In our public code, users can find our pre-trained weights so that they can perform fine-tuning in any future system building from this one.

## 5 Results

### 5.1 State of the art comparison

In this section we compare our final results to the current state of the art for image classification in the CIFAR-10, CIFAR-100 and DVS-CIFAR10 datasets. As noted in [24], most previous works train on the training set, evaluate the

Table 4. Image classification test performance on CIFAR-100. S-Resnet38 stands for the architecture defined in Section 3.2.2 with  $n = 6$  and 16 base filters. Wider architectures use 32 base filters and "boosting" indicates the use of a boosting layer (Section 3.2.3). Wider architectures trained for 70 epochs, regular architectures trained for 200 epochs.

Network	Parameters	CIFAR-100 Acc
S-ResNet38	639,760	68.71 %
S-ResNet38 + boosting	697,360	64.6 %
S-ResNet38_wider	2,399,776	74.46 %
S-ResNet38_wider + boosting	2,514,976	73.21 %

Table 5. Image classification test performance on CIFAR-100. Except for the learnable leak factor, both architectures and training procedures are identical. Trained for 200 epoch.

Network	CIFAR-100 Accuracy
S-ResNet38 LIF	68.71 %
S-ResNet38 Parametric LIF	64.93 %

Table 6. Optimal leak coefficient for ResNet38 in CIFAR-100 obtained through two different methods (A single coefficient shared by all layers). "Hyperparameter search" uses BOHB algorithm to optimize the parameter. The value for this method corresponds to the mean among the 6 best performing configurations found with its corresponding standard deviation in parenthesis. "Learned through PLIF" learns the value by backpropagation during training, the value corresponds to the result after 70 epochs of training.

Method	Leak coefficient
Hyper-parameter search	0.889 ( $\pm$ 0.003)
Learned through PLIF	0.986

Table 7. Image classification test performance on CIFAR-100. In "S-ResNet38\_wider + Boost Single PLIF" one single leak value is learned for all layers. Except for the learnable leak factor, both architectures and training procedures are identical. Trained for 70 epoch.

Network	CIFAR-100 Acc
S-ResNet38_wider + Boost LIF	73.21 %
S-ResNet38_wider + Boost Single PLIF	72.44 %

Table 8. Image classification test performance on CIFAR-100. Except for the spike generation process, both architectures and training procedures are identical. Trained for 100 epoch.

Network	CIFAR-100 Accuracy
S-ResNet38 Poisson spike generation	64.96 %
S-ResNet38 Raw image	69.03 %

Table 9. Image classification test performance on DVS CIFAR-10. Pre-train column indicates if the network was trained from scratch or pre-trained with a certain dataset. S-Resnet38 stands for the architecture defined in Section 3.2.2 with  $n = 6$  and 16 base filters. Wider architectures use 32 base filters and "boosting" indicates the use of a boosting layer (Section 3.2.3). Trained for 70 epochs.

Network	Pre-train	DVS CIFAR-10 Acc
S-ResNet38	No	63.3 %
S-ResNet38	CIFAR-100	70.4 %
S-ResNet38_wider + boosting	No	65.5 %
S-ResNet38_wider + boosting	CIFAR-100	69.8 %

Table 10. Image classification test performance on CIFAR-10. Pre-train column indicates if the network was trained from scratch or pre-trained with a certain dataset. S-Resnet38 stands for the architecture defined in Section 3.2.2 with  $n = 6$  and 16 base filters. Wider architectures use 32 base filters and "boosting" indicates the use of a boosting layer (Section 3.2.3). S-Resnet38 Trained for 200 epochs from scratch and for 100 when fine-tuned. Wider architectures trained for 70 epochs.

Network	Pre-train	CIFAR-10 Acc
S-ResNet38	No	90.82 %
S-ResNet38	CIFAR-100	92.44 %
S-ResNet38_wider + boosting	No	93.77 %
S-ResNet38_wider + boosting	CIFAR-100	93.59 %



test set at each step, and then report the highest test accuracy obtained. We consider this approach to be reporting validation accuracy rather than test. In our setup, we evaluate the test set after all the training epochs, without using its value for tuning the training. We also evaluate validation accuracy in the same manner than the previous methods in order to make a fair comparison.

The developed S-ResNet outperforms all previous SNN methods in classification accuracy for the CIFAR-10 and CIFAR-100 datasets (Table 11). In the DVS-CIFAR10 dataset, we find that the validation accuracy for the best performing network outperforms ours, but when measuring test score, ours is superior.

Before our work, in the CIFAR-10 dataset, the most accurate network was a conversion method. These new results prove how directly training an SNN can perform better without the need of imitating non-spiking computations.

Moreover, in Table 12 we compare the performance of the original ANN ResNet to our S-ResNet. We compare the version without boosting and with 16 base filters, as that is the same architecture the original paper used. We can see how the performance on the trained SNN is not far from its non-spiking counterpart, demonstrating how improvements in SNN training can push these technologies to comparable levels with conventional deep learning.

Comparing to the previous trainable SNN architectures, our network uses many less parameters. Fig. 3, 4 and 5 show a map of the accuracy versus the number of parameters. The main cause for the difference in parameters is that our network has a smaller number of channels in convolutional layers and only a single fully-connected layer. Then, even when our network is deeper than the others, it is actually lighter in terms of synaptic connections.

## 5.2 The latency - accuracy compromise

Apart from raw accuracy, the efficiency of algorithms is a major factor when deploying systems in the real world. For image classification in SNN, the amount of time-steps used for prediction regulates a trade-off between accuracy and time or volume of computations.

In order to elucidate the effect of this trade-off in our system, in Table 13 we present the accuracy of S-ResNet38 with different numbers of time-steps. Starting from our best network trained with 50 time-steps, we test how the accuracy degrades when dropping the last 10/20/30/40 steps. Additionally, we compare this to the result obtained by directly training with less time-steps.

The results show how for CIFAR-100, the network trained with 20 steps performs better than dropping the last 30 steps of a 50-step network. Still this same experiment in the CIFAR-10 dataset shows the opposite results by a close margin, indicating that the 50-step network had a

Table 11. Image classification validation performance on CIFAR-10, CIFAR-100 and DVS-CIFAR10. Our S-Resnet38 in CIFAR-10 and CIFAR-100 stands for the wider version of the architecture defined in Section 3.2.2 with  $n = 6$ , 32 base filters, and boosting layer. In DVS-CIFAR10 we use the 16 filters version without boosting and with the pre-training step.

Network	Method	Dataset	Accuracy
Kim [15] S-VGG9	Spiking BP	CIFAR-10	90.05 %
Lee [21] S-ResNet11	Spiking BP	CIFAR-10	90.95 %
Zheng [23] S-ResNet19	Spiking BP	CIFAR-10	93.15 %
Fang [24] CifarNet	Spiking BP	CIFAR-10	93.50%
Sengupta [33] VGG-16	SNN conversion	CIFAR-10	91.55%
Stockl [12] ResNet50	SNN conversion	CIFAR-10	92.42%
Han [11] VGG16	SNN conversion	CIFAR-10	93.63%
<b>Ours S-ResNet38</b>	<b>Spiking BP</b>	<b>CIFAR-10</b>	<b>94.10%</b>
Kim [15] S-VGG9	Spiking BP	CIFAR-100	66.6 %
Han [11] VGG16	SNN conversion	CIFAR-100	70.97%
<b>Ours S-ResNet38</b>	<b>Spiking BP</b>	<b>CIFAR-100</b>	<b>74.46%</b>
Kim [15] S-VGG9	Spiking BP	DVS-CIFAR10	63.2 %
Zheng [23] S-ResNet19	Spiking BP	DVS-CIFAR10	67.8 %
Fang [24] CifarDVSNet	Spiking BP	DVS-CIFAR10	74.8%
<b>Ours S-ResNet38</b>	<b>Spiking BP</b>	<b>DVS-CIFAR10</b>	<b>71.3%</b>

Table 12. Image classification performance on CIFAR-10 comparing the original ANN ResNet results to our S-ResNet. S-Resnet38 stands for the architecture defined in Section 3.2.2 with  $n = 6$  and 16 base filters.

Network	Method	CIFAR-10 Accuracy
ResNet32 [27]	ANN	92.49 %
ResNet44 [27]	ANN	92.83 %
S-ResNet38	SNN	90.94 %

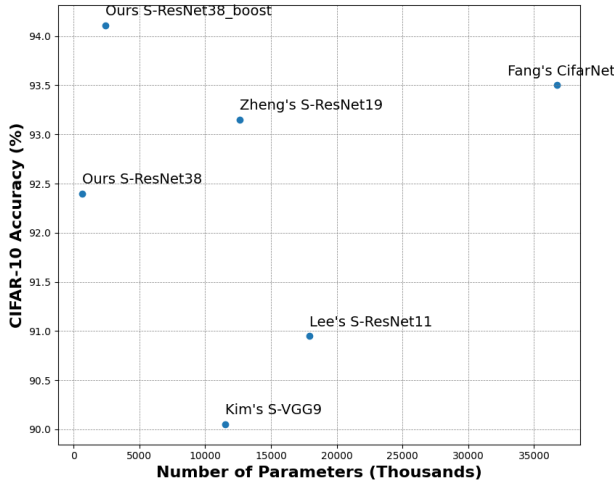


Figure 3. CIFAR-10 accuracy versus number of parameters. We compare our network to the best performing trainable SNNs and the other spiking ResNets. "S-ResNet38\_boost" uses the wider architecture with 32 base filters. The number of parameters for other works was counted using their publicly available code.

more complete training.

At 10 steps, the degrading of the 50-step network becomes more obvious. Interestingly the network trained with 20 time-steps does not degrade as much, as it is only losing half of its computations and therefore still managing to extract the core visual features.

Finally, we hypothesise that the optimal leakage coefficient for the neurons might be correlated to the amount of time-steps the network is ran for. Given that the leak factor that we use was obtained through the hyper-parameter search process, and given that this process prioritized large amounts of time-steps, we believe the optimal leak factor for 20-step inferences could be different from the one we are using. We empirically test this by training the network again with PLIF neurons, a process that allows us to optimize the leak value in a single training run. The results, as seen in Table 14, prove how we obtain a better performance when the leak coefficient is optimized for the number of inference steps, confirming our hypothesis.

From this study we learn how the optimal solution is to perform training with the same amount of time-steps that we want to target at inference time and to optimize hyper-parameters such as the leak factor for this same objective. Still, our SNNs can withstand the effect of early stopping, retaining most of their accuracy even when big percentages of their computation steps are dropped. This allows to pro-

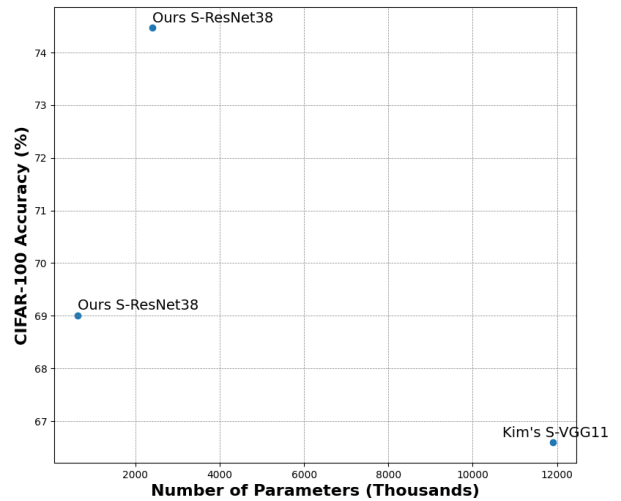


Figure 4. CIFAR-100 accuracy versus number of parameters. We compare our network to the best performing trainable SNN in this dataset. The two results for S-ResNet38 correspond to the same network with 16 or 32 base filters (where 32 base filters has more parameters than 16). The number of parameters for other works was counted using their publicly available code.

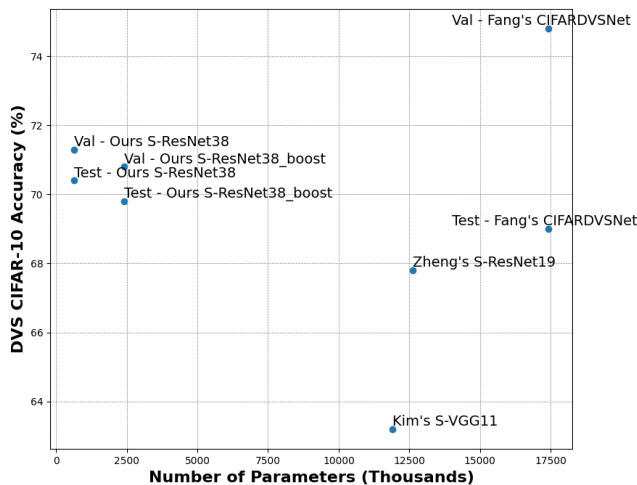


Figure 5. DVS CIFAR-10 accuracy versus number of parameters. We compare our network to the best performing trainable SNNs and the other spiking ResNets. The number of parameters for other works was counted using their publicly available code. The "Val" prefix stands for validation accuracy while "Test" stands for testing accuracy.

Table 13. Influence of the number of time-steps in the validation accuracy. Results of the evaluation of the best performing S-ResNet38 with boosting. Training time-steps specifies the number of steps used during training, inference time-steps the steps used for inference. If the inference number is smaller than the training one, early stopping is applied and the last  $N$  time-steps (and learned BNTT layers) are not used. For comparison, the training is reproduced also with 20 time-steps. Clarification: The architecture is the same but the results for CIFAR-100 use the weights trained in CIFAR-100 and the CIFAR-10 results use the weights trained in CIFAR-10.

Inference t-steps	Training t-steps	CIFAR-100 Acc	CIFAR-10 Acc
50	50	73.40 %	94.10 %
40	50	73.14 %	93.96 %
30	50	71.75 %	93.61 %
20	50	65.78 %	91.93 %
20	20	67.70 %	91.28 %
10	50	15.15 %	63.86 %
10	20	62.28 %	90.45 %

Table 14. CIFAR-10 validation accuracy for inferences of 20 time-steps. The first network was trained with 50 time-steps in training time, the others were trained with 20 time-steps. The first two networks use the leak value learned through hyper-parameter optimization done for the 50-step network. The third one optimizes the leak value during its training through PLIF neurons.

Leak factor	Inference t-steps	Training t-steps	CIFAR-10 Acc
0.874	20	50	91.93 %
0.874	20	20	91.28 %
0.995	20	20	92.8 %

vide early estimates in time sensible tasks or to reduce computational cost.

## 6 Conclusions

In this paper we presented a study on several aspects of the SNN design process and we provided empirical results that allow to make informed choices when designing a new SNN feature extractor. Using this knowledge a new SNN architecture was proposed which outperforms previous approaches.

Additionally, these results demonstrate how SNNs do not need to use conversion methods in order to maximize their accuracy while pushing their performance closer to that of non-spiking deep learning.

We believe this work can be regarded as an incremental contribution to the research on SNN feature extractors. We

provide our code and pre-trained weights so that more experiments can follow this study and new applications can benefit of increased accuracy by fine tuning our networks.

## Acknowledgement

This work was supported by the US Air Force Office of Scientific Research under Grant for project FA8655-20-1-7037

The contents were approved for public release under case AFRL-2021-3889 and they represent the views of only the authors and does not represent any views or positions of the Air Force Research Laboratory, US Department of Defense, or US Government.

## References

- [1] Mike Davies, Narayan Srinivasa, Tsung-Han Lin, Gautham China, Yongqiang Cao, Sri Harsha Choday, Georgios Dimou, Prasad Joshi, Nabil Imam, Shweta Jain, et al. Loihi: A neuromorphic manycore processor with on-chip learning. *Ieee Micro*, 38(1):82–99, 2018.
- [2] Andrew S Cassidy, Paul Merolla, John V Arthur, Steve K Esser, Bryan Jackson, Rodrigo Alvarez-Icaza, Pallab Datta, Jun Sawada, Theodore M Wong, Vitaly Feldman, et al. Cognitive computing building block: A versatile and efficient digital neuron model for neurosynaptic cores. In *The 2013 International Joint Conference on Neural Networks (IJCNN)*, pages 1–10. IEEE, 2013.
- [3] Mike Davies, Andreas Wild, Garrick Orchard, Yulia Sandamirskaya, Gabriel A Fonseca Guerra, Prasad Joshi, Philipp Plank, and Sumedh R Risbud. Advancing neuromorphic computing with loihi: A survey of results and outlook. *Proceedings of the IEEE*, 109(5):911–934, 2021.
- [4] Lasse F Wolff Anthony, Benjamin Kanding, and Raghavendra Selvan. Carbontracker: Tracking and predicting the carbon footprint of training deep learning models. *arXiv preprint arXiv:2007.03051*, 2020.
- [5] Yann LeCun, Yoshua Bengio, and Geoffrey Hinton. Deep learning. *nature*, 521(7553):436–444, 2015.
- [6] Steven K Esser, Paul A Merolla, John V Arthur, Andrew S Cassidy, Rathinakumar Appuswamy, Alexander Andreopoulos, David J Berg, Jeffrey L McKinstry, Timothy Melano, Davis R Barch, et al. Convolutional networks for fast, energy-efficient neuromorphic computing. *Proceedings of the national academy of sciences*, 113(41):11441–11446, 2016.
- [7] Alexander Kugele, Thomas Pfeil, Michael Pfeiffer, and Elisabetta Chicca. Efficient Processing of Spatio-Temporal Data Streams With Spiking Neural Networks. *Frontiers in Neuroscience*, 14(May):1–13, 2020.
- [8] Christoph Stöckl and Wolfgang Maass. Recognizing images with at most one spike per neuron. *arXiv preprint arXiv:2001.01682*, 2019.
- [9] Emre O Neftci, Hesham Mostafa, and Friedemann Zenke. Surrogate gradient learning in spiking neural networks: Bringing the power of gradient-based optimization to spiking neural networks. *IEEE Signal Processing Magazine*, 36(6):51–63, 2019.
- [10] Bing Han, Gopalakrishnan Srinivasan, and Kaushik Roy. Rmp-snn: Residual membrane potential neuron for enabling deeper high-accuracy and low-latency spiking neural network. In *Proceedings of the IEEE/CVF Conference on Computer Vision and Pattern Recognition*, pages 13558–13567, 2020.
- [11] Bing Han and Kaushik Roy. Deep spiking neural network: Energy efficiency through time based coding. In *Computer Vision–ECCV 2020: 16th European Conference, Glasgow, UK, August 23–28, 2020, Proceedings, Part X 16*, pages 388–404. Springer, 2020.
- [12] Christoph Stöckl and Wolfgang Maass. Optimized spiking neurons can classify images with high accuracy through temporal coding with two spikes. *Nature Machine Intelligence*, 3(3):230–238, 2021.
- [13] Lei Deng, Yujie Wu, Xing Hu, Ling Liang, Yufei Ding, Guoqi Li, Guangshe Zhao, Peng Li, and Yuan Xie. Rethinking the performance comparison between SNNs and ANNs. *Neural Networks*, 121:294–307, 2020.
- [14] Yujie Wu, Lei Deng, Guoqi Li, Jun Zhu, and Luping Shi. Spatio-temporal backpropagation for training high-performance spiking neural networks. *Frontiers in neuroscience*, 12:331, 2018.
- [15] Youngeun Kim and Priyadarshini Panda. Revisiting batch normalization for training low-latency deep spiking neural networks from scratch. *arXiv preprint arXiv:2010.01729*, 2020.
- [16] Dongsung Huh and Terrence J Sejnowski. Gradient descent for spiking neural networks. In S. Bengio, H. Wallach, H. Larochelle, K. Grauman, N. Cesa-Bianchi, and R. Garnett, editors, *Advances in Neural Information Processing Systems*, volume 31. Curran Associates, Inc., 2018.
- [17] Hesham Mostafa and Gert Cauwenberghs. A learning framework for winner-take-all networks with stochastic synapses. *Neural computation*, 30(6):1542–1572, 2018.
- [18] Hesham Mostafa. Supervised learning based on temporal coding in spiking neural networks. *IEEE transactions on neural networks and learning systems*, 29(7):3227–3235, 2017.
- [19] Jacques Kaiser, Hesham Mostafa, and Emre Neftci. Synaptic plasticity dynamics for deep continuous local learning (decolle). *Frontiers in Neuroscience*, 14:424, 2020.
- [20] Łukasz Kuśmierz, Takuya Isomura, and Taro Toyoizumi. Learning with three factors: modulating hebbian plasticity with errors. *Current opinion in neurobiology*, 46:170–177, 2017.
- [21] Chankyu Lee, Syed Shakib Sarwar, Priyadarshini Panda, Gopalakrishnan Srinivasan, and Kaushik Roy. Enabling spike-based backpropagation for training deep neural network architectures. *Frontiers in neuroscience*, 14:119, 2020.

- [22] S. Shrestha and Garrick Orchard. Slayer: Spike layer error reassignment in time. In *NeurIPS*, 2018.
- [23] Hanle Zheng, Yujie Wu, Lei Deng, Yifan Hu, and Guoqi Li. Going deeper with directly-trained larger spiking neural networks. *arXiv preprint arXiv:2011.05280*, 2020.
- [24] Wei Fang, Zhaofei Yu, Yanqi Chen, Timothée Masquelier, Tiejun Huang, and Yonghong Tian. Incorporating learnable membrane time constant to enhance learning of spiking neural networks. In *Proceedings of the IEEE/CVF International Conference on Computer Vision*, pages 2661–2671, 2021.
- [25] Wei Fang, Zhaofei Yu, Timothée Masquelier, Yanqi Chen, Tiejun Huang, and Yonghong Tian. Spike-based residual blocks. *arXiv preprint arXiv:2102.04159*, 2021.
- [26] Karen Simonyan and Andrew Zisserman. Very deep convolutional networks for large-scale image recognition. In Yoshua Bengio and Yann LeCun, editors, *3rd International Conference on Learning Representations, ICLR 2015, San Diego, CA, USA, May 7-9, 2015, Conference Track Proceedings*, 2015.
- [27] Kaiming He, Xiangyu Zhang, Shaoqing Ren, and Jian Sun. Deep residual learning for image recognition. In *Proceedings of the IEEE conference on computer vision and pattern recognition*, pages 770–778, 2016.
- [28] Larry F Abbott. Lapicque’s introduction of the integrate-and-fire model neuron (1907). *Brain research bulletin*, 50(5-6):303–304, 1999.
- [29] Tim Cooijmans, Nicolas Ballas, César Laurent, Çağlar Gülçehre, and Aaron Courville. Recurrent batch normalization. *arXiv preprint arXiv:1603.09025*, 2016.
- [30] Adam Paszke, Sam Gross, Francisco Massa, Adam Lerer, James Bradbury, Gregory Chanan, Trevor Killeen, Zeming Lin, Natalia Gimelshein, Luca Antiga, et al. Pytorch: An imperative style, high-performance deep learning library. *Advances in neural information processing systems*, 32:8026–8037, 2019.
- [31] Wei Fang, Yanqi Chen, Jianhao Ding, Ding Chen, Zhaofei Yu, Huihui Zhou, and Yonghong Tian. and other contributors. spikingjelly, 2020.
- [32] Stefan Falkner, Aaron Klein, and Frank Hutter. Bohb: Robust and efficient hyperparameter optimization at scale. In *International Conference on Machine Learning*, pages 1437–1446. PMLR, 2018.
- [33] Abhronil Sengupta, Yuting Ye, Robert Wang, Chiao Liu, and Kaushik Roy. Going deeper in spiking neural networks: Vgg and residual architectures. *Frontiers in neuroscience*, 13:95, 2019.